

https://dspace.org/

Fracture Mechanics Analyses Of Static And Dynamic Failures Associated With Welding

Boothroyd, Colin Allistair

2015-01-09
http://hdl.handle.net/10539/16336

Downloaded from a DSpace repository. https://dspace.org/

crack depth (a/t) increases, whereas the aspect ratio of a crack under bending loads (Figure 6.1 (b)) tends to 0 as the fractional crack depth increases. Although this is not expected to invalidate the stress intensity factor calculation, it will cause a variability between the stress intensity for the two cases of tension and bending for a given crack depth and applied stress, since this is uniquely defined by the specific values of a and 2c. Moreover, the rate of change of crack depth (da/dN), at a given crack depth, will be different for the two cases.

The method used for calculating stress intensities in fillet welded speciomens (128-130) only evaluates the conditions at the deepest part of the crack. Solutions have been published (see, for example, reference 126) for the stress intensity at the surface, but these are only valid for plain plate specimens. Thus, the rate of change of surface length (d2c/dN) is plotted against the corresponding rates of change of crack depth (da/dN) in Figure 6.15, and it can be seen that the rate of change of surface length is an order of magnitude greater than the rate of change of crack depth. This is consistent with the semi-elliptical shapes developed in these specimens.

It was initially intended that the crack shape development data (ie a/2c versus a/t or a versus 2c) would be used, in conjunction with the change of potential drop with crack depth, to estimate crack depths and crack lengths continuously during propagation. The crack tip stress intensity would then be calculated for these small increments of growth (eg every μV change in potential), and this would yield a continuous da/dN versus ΔK for a particular test, without changing the stress conditions to mark the crack front.

However, as seen in Figures 6.10 and 6.12, there was some considerable scatter in the experimental correlations. In order to evaluate the effect of this scatter on the proposed method of monitoring the crack growth and continuously calculating the crack tip stress intensities, the potential drop readings obtained during the testing of one particular specimen were used to extrapo

for values of crack depth, from Figure 6.12. For each potential drop reading, three crack depths were obtained, corresponding to the mean regression value, and the two outer limits of the experimental scatterband. For each of these three crack depths, three surface lengths were obtained from the experimental data shown in Figure 6.10, and the stress intensity of each of the nine possible defect shapes were evaluated, using the method described in Section 6.1.3. Thus, for each potential drop reading, three predicted values of crack growth rate (da/dN) were calculated, and for each of these three growth rates, three cyclic stress intensities ($\triangle K$) were evaluated. In addition, of course, the "true" da/dN and $\triangle K$ were evaluated from the beachmarked fracture surface. The results of this exercise, shown in Figure 6.16, indicate that the scatter observed in the correlation of potential drop with crack depth, and of crack depth with crack length give significant errors in the evaluation of the crack tip stress intensity. In Figure 6.16 the three sets of data are represented by different symbols, and for further clarity, the "true" data point of each set is represented by a solid symbol.

However, the results obtained in the evaluation of da/dN and $\triangle K$ from the beachmarked specimens gave sufficient information for the purposes of evaluating crack growth rates, in this particular investigation. Indeed, all the results described in this Chapter were of considerable value in the investigation of the fatigue behaviour of various fillet weld details. This experimental test programme was aimed at establishing the 10 million cycle endurance limit of non-load-carrying fillet welds, and evaluating the effects of weld procedure and post-weld dressing techniques on this endurance limit. The identification of the crack initiation sites indicated the need for weld dressing procedures to be implemented, such that the weld toe profile was modified, and the preferential crack initiation site was either removed or placed in a state of compressive residual stress. This resulted in fatigue cracks initiating at higher applied stress levels, remote from the weld toe. Identification of the crack initiation site in the dressed specimens served to indicate whether or not the dressing had been effectively carried out. The evaluation of the crack shape development was

essential in the calculation of crack growth rates and crack tip stress intensity factors. Thus, these macroscopic features could also be used, in a qualitative manner, in the investigation of service fatigue failures.

6.4 Summary

This Chapter has reviewed the features observed in the macroscopic examination of the fatigue fracture surfaces of the specimen weldments. These features were used to substantiate the results obtained in the investigation of the fatigue behaviour of non-load-carrying fillet welds, described in the preceding Chapter.

It was shown that initiation typically occurs subsurface, at the root of the weld, in the stitch welded samples although there were some instances of crack initiation from the weld ends.

Consistent with previous published work (12,13), the presence of weld toe undercut in the continuous specimens causes a drastic reduction in the fatigue strength of this detail. In the absence of undercut, multiple initiation occurs from the weld toe, and this required much higher stress ranges. If these preferential crack initiation sites are removed by post-weld mechanical dressing, the crack initiation site is removed from the weld toe to the weld root with a corresponding increase in the fatigue strength. However, initiation can occur from the weld toe if defects remain there after the grinding or peening, indicating that some care is needed for the successful implementation of these improvement techniques. On the other hand, initiation can occur from the flame cut edge of the main load bearing plate, remote from the dressed welds.

Heat-tinting and beachmarking techniques were used to locate the successive positions of the crack front during propagation. It was shown that the shape of the cracks developed in the as-welded specimens is subject to some variability due to the different initiating defect shapes. However, the cracks tended to

essential in the calculation of crack growth rates and crack tip stress intensity factors. Thus, these macroscopic features could also be used, in a qualitative manner, in the investigation of service fatigue failures.

6.4 Summary

This Chapter has reviewed the features observed in the macroscopic examination of the fatigue fracture surfaces of the specimen weldments. These features were used to substantiate the results obtained in the investigation of the fatigue behaviour of non-load-carrying fillet welds, described in the preceding Chapter.

It was shown that initiation typically occurs subsurface, at the root of the weld, in the stitch welded samples although there were some instances of crack initiation from the weld ends.

Consistent with previous published work (12,13), the presence of weld toe undercut in the continuous specimens causes a drastic reduction in the fatigue strength of this detail. In the absence of undercut, multiple initiation occurs from the weld toe, and this required much higher stress ranges. If these preferential crack initiation sites are removed by post-weld mechanical dressing, the crack initiation site is removed from the weld toe to the weld root with a corresponding increase in the fatigue strength. However, initiation can occur from the weld toe if defects remain there after the grinding or peening, indicating that some care is needed for the successful implementation of these improvement techniques. On the other hand, initiation can occur from the flame cut edge of the main load bearing plate, remote from the dressed welds.

Heat-tinting and beachmarking techniques were used to locate the successive positions of the crack front during propagation. It was shown that the shape of the cracks developed in the as-welded specimens is subject to some variability due to the different initiating defect shapes. However, the cracks tended to

the semi-elliptical equilibrium shape expected for this geometry and loading arrangement. In the ground and peened specimens, on the other hand, multiple crack propagation occurs, this growth pattern was established by stopping selected specimens at different stages after initiation had occurred.

Both the potential drop and the compliance methods were evaluated for use as crack monitoring techniques. However, it is necessary to mark the crack front during propagation in order to calibrate these methods, and this affected the correlation between specimen compliance and crack depth. The potential drop technique is inherently innacurate for this specimen geometry, especially during the initial growth stages. Thus, it was not possible to use the potential drop, or the compliance method to evaluate crack growth rates and crack tip stress intensities continuously during testing.

However, the results from the beach-marked specimens indicated that the cyclic stress intensity at the crack tip (at the deepest point of the crack front) ranged between 5 and 30 MPa $\sqrt{m}$, depending on the crack depth and applied stress level, and this corresponded to rates of change of crack depth of between 3×10^{-10} and 7×10^{-9} m/cycle.

Finally, it was shown that the rate of change of crack length was an order of magnitude faster than the rate of change of crack depth; this is consistent with the semi-elliptical equilibrium crack shape.

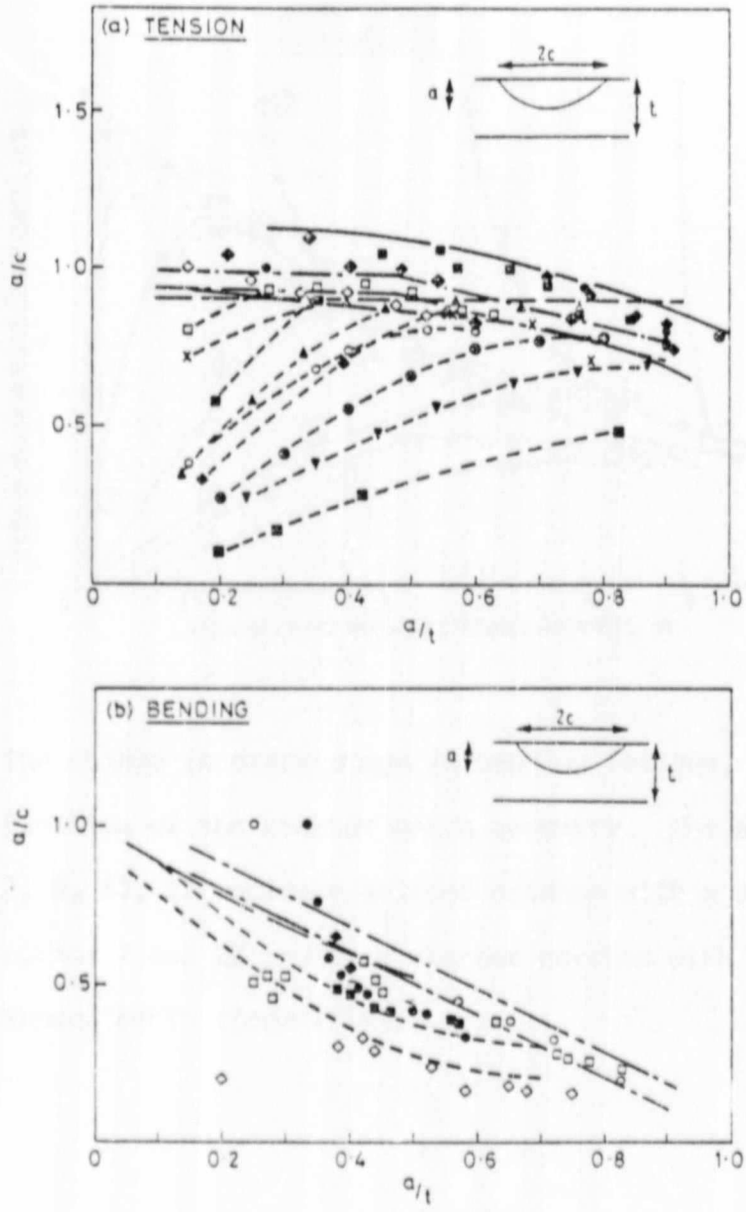


Figure 6.1 The development of crack shape under (a) direct tension and (b) pure bending. The different symbols refer to various data sources (see reference 115).

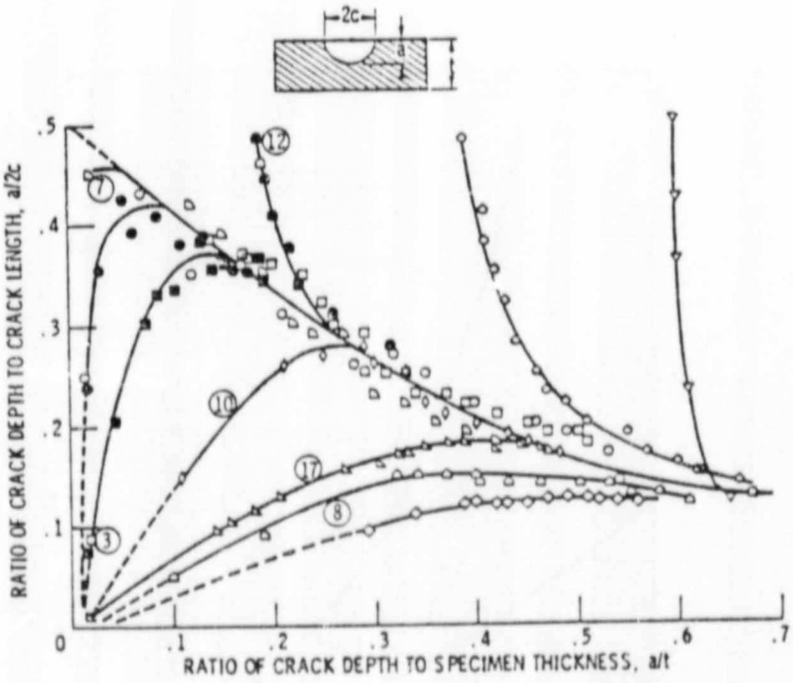


Figure 6.2 The change in crack shape in bending fatigue, as a function of the starter notch geometry. The numbers 3, 8, 10, 17 indicate starter notches with a small aspect ratio; 7 and 12 indicate starter notches with a large aspect ratio (from (119)).

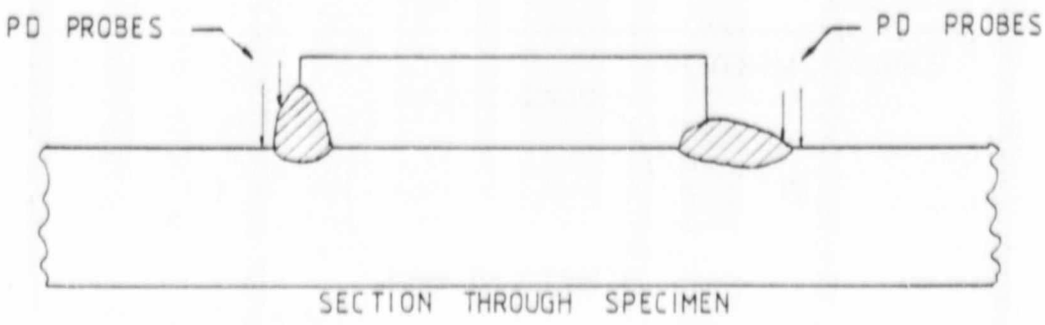


Figure 6.3 An illustration of the problems associated with obtaining reproducible electrical spacings in welded specimens (from (123)). Note that the weld shape is exaggerated for clarity.

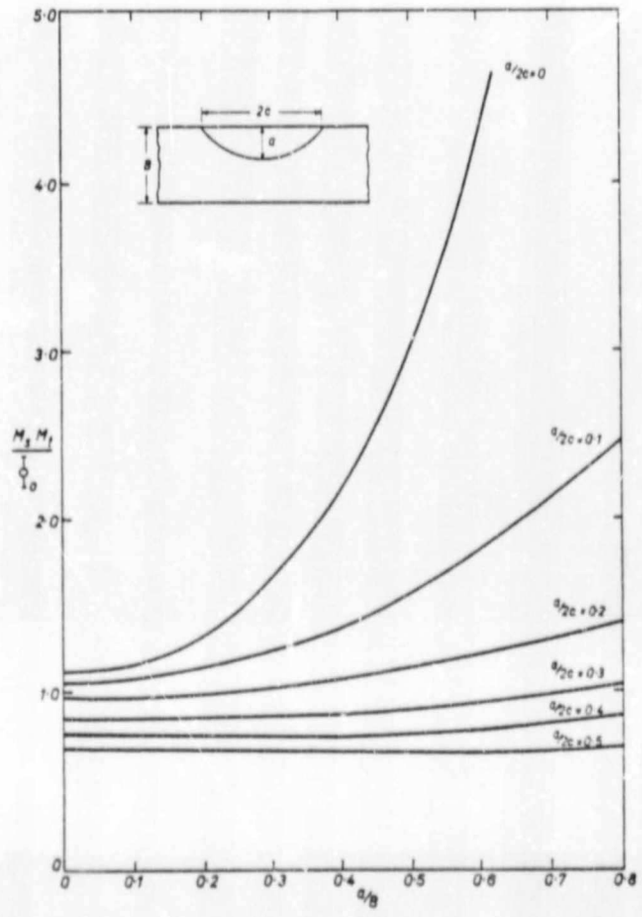


Figure 6.4 Variation of the magnification factor with crack depth for various surface-crack shapes (from (128)).

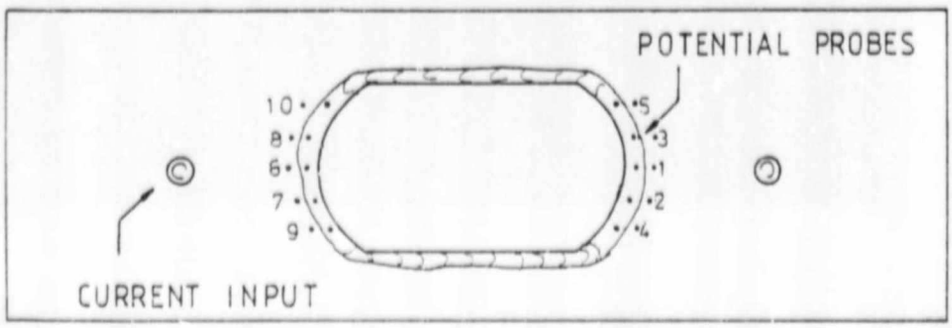
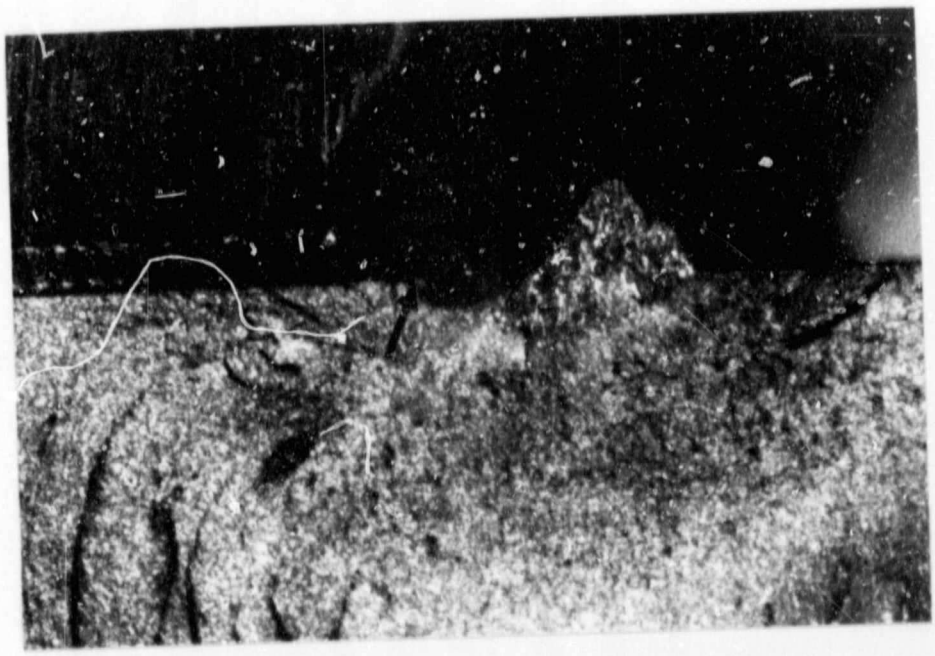


Figure 6.5 The current input and potential drop positions used in this work.



(a)



(b)

Figure 6.6 Crack initiation from (a) the weld root and (b) the weld toe in the stitch welded samples. Magnification 5x.

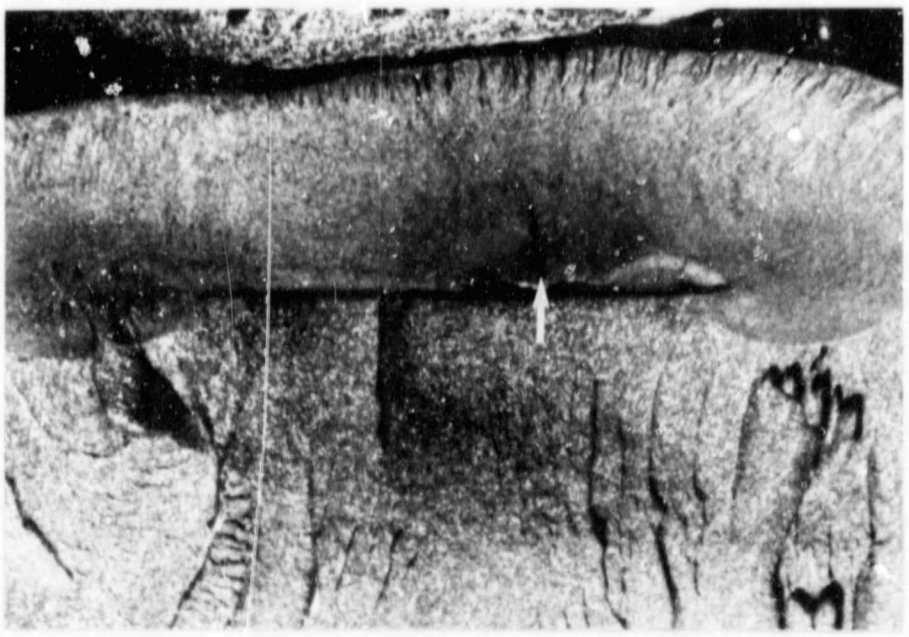


(a)

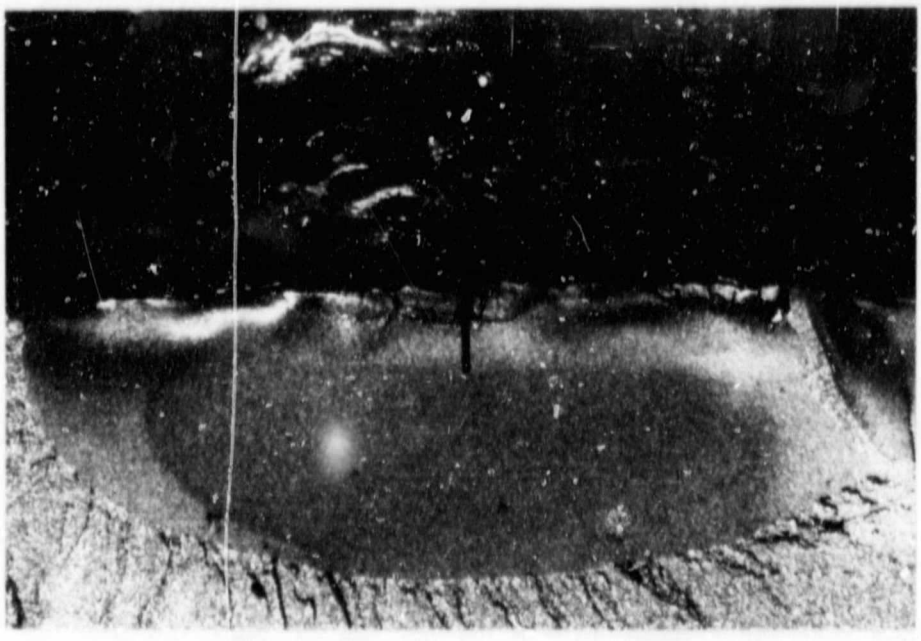


(b)

Figure 6.7 Crack initiation in the continuous welds from (a) multiple points along the weld toe and (b) from an undercut defect. Magnification 5x.



(a)



(b)

Figure 6.8 Crack initiation in the dressed specimens from (a) the weld root and (b) the weld toe. Magnification 4x.

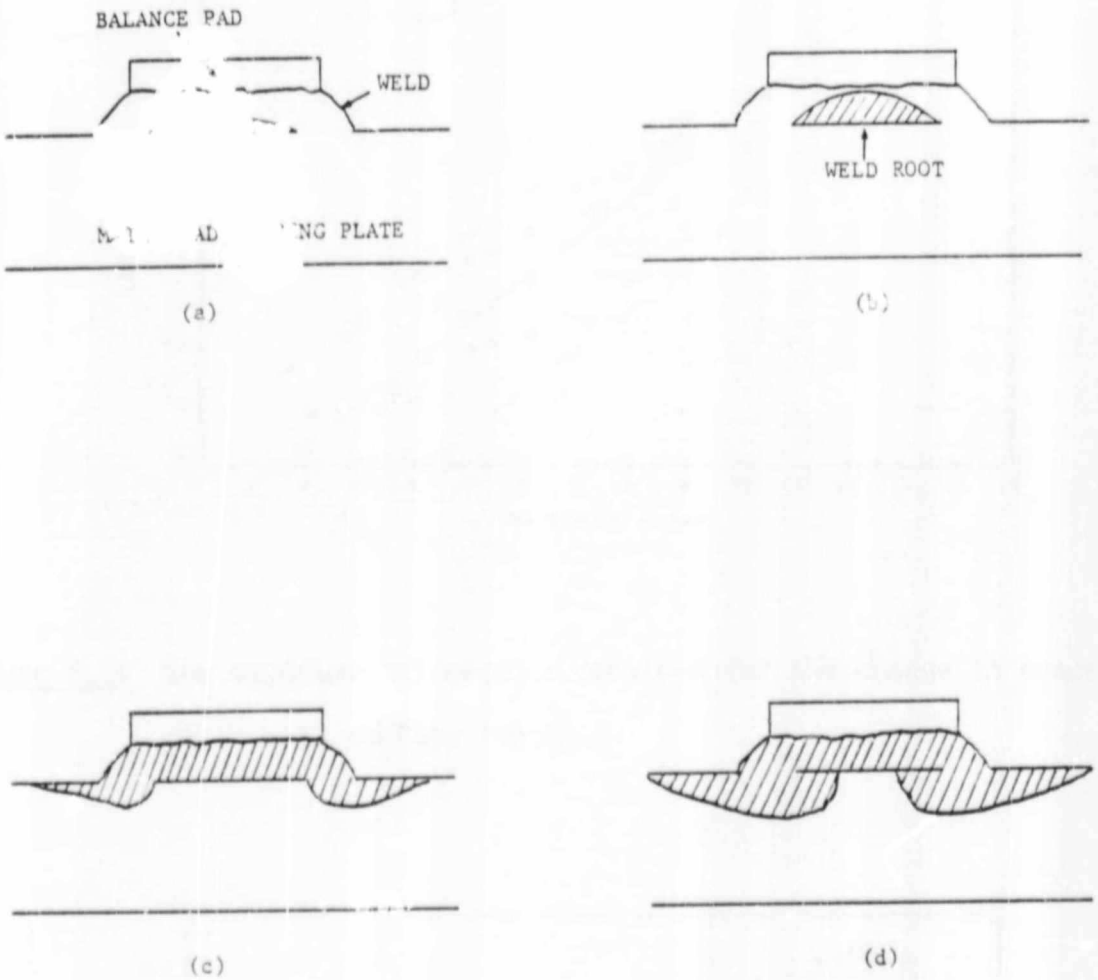


Figure 6.9 Schematic representation of the stages in crack propagation in the ground and peened specimens (a) initiation from weld root, (b) propagation upwards to the surface of the weld, (c) propagation downwards from the side welds and (d) propagation downwards and across the main load bearing plate. (Not to scale).

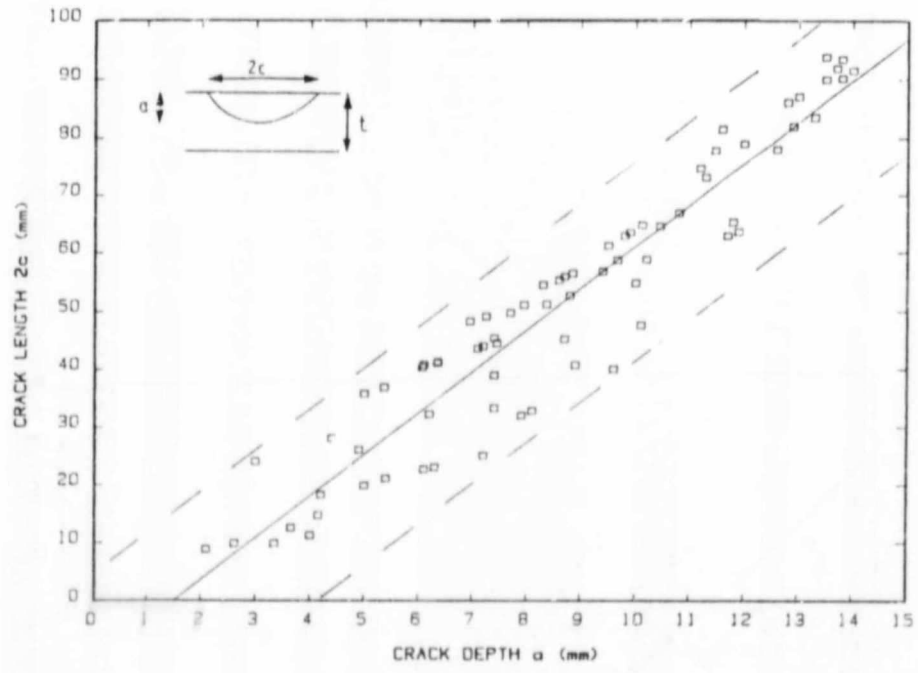


Figure 6.10 The experimental results obtained for the change in crack depth with surface length.

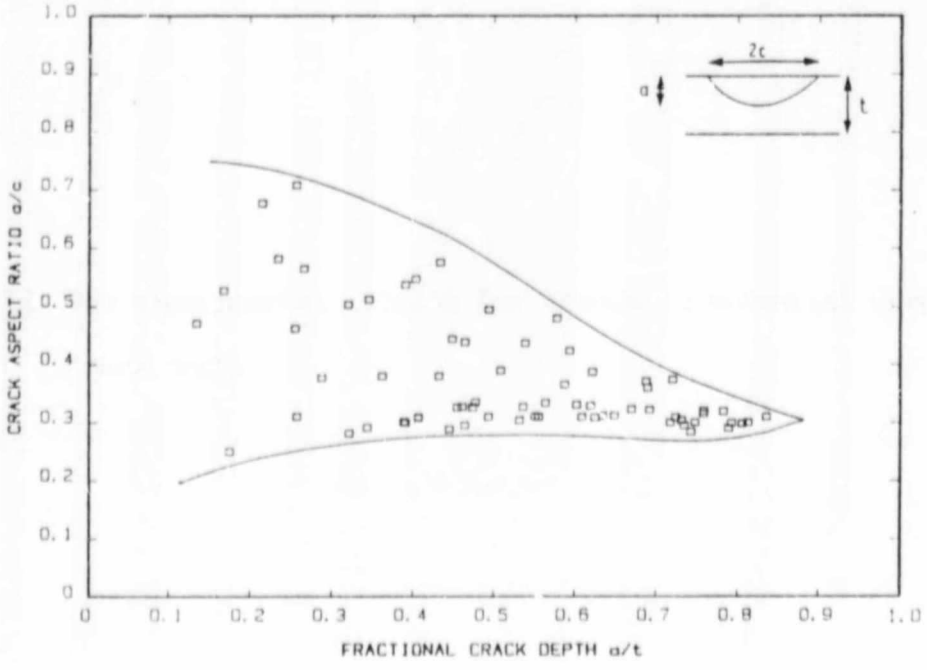


Figure 6.11 The experimental results obtained for the change in crack aspect ratio with fractional crack depth.

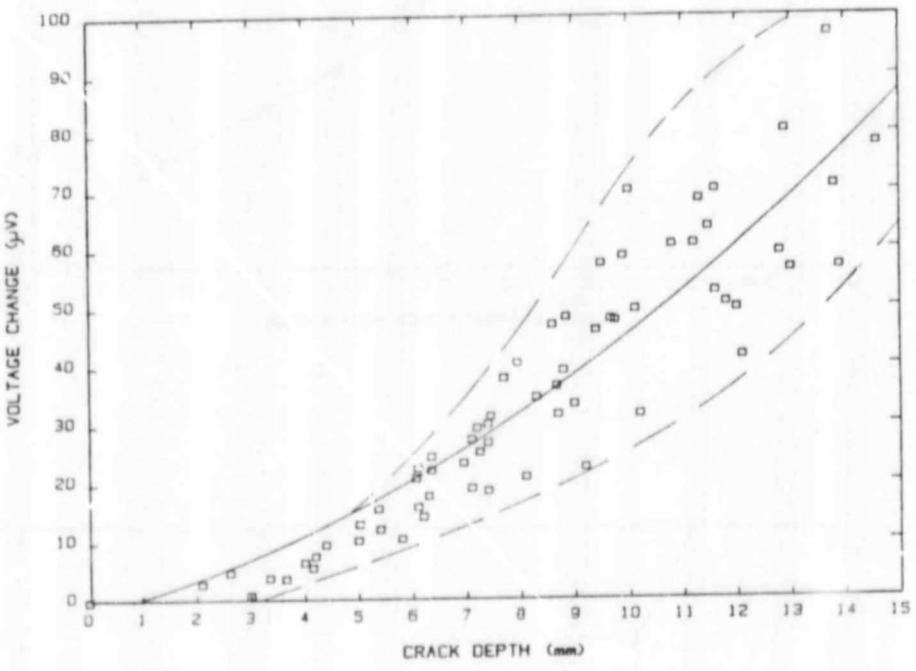
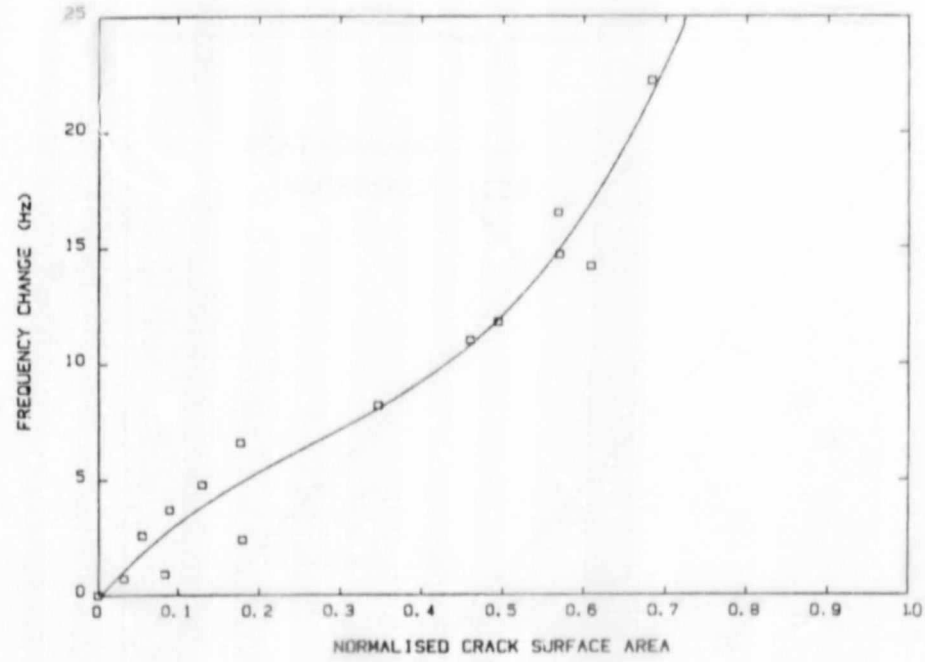
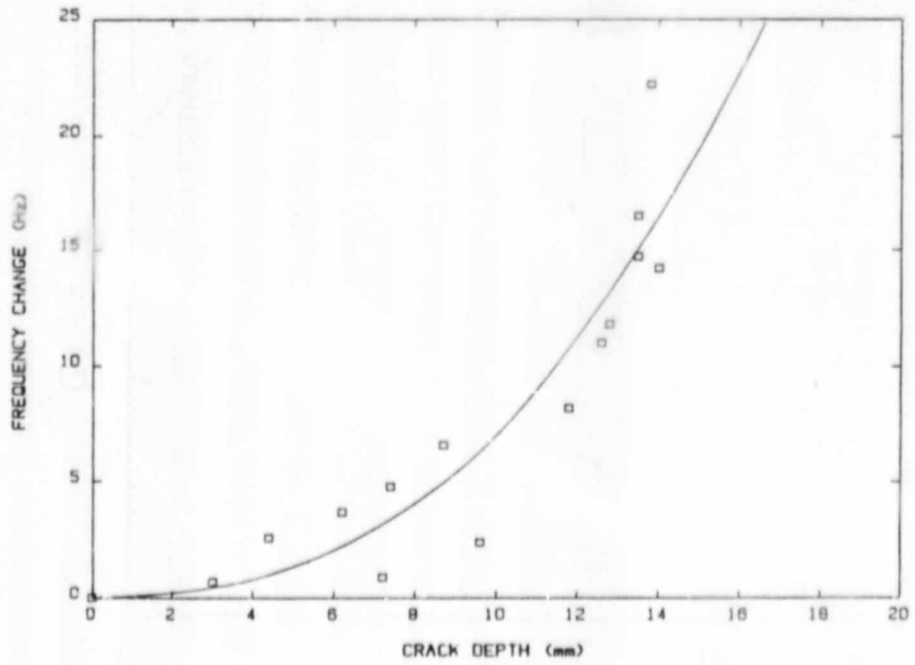


Figure 6.12 The experimental results for change in potential drop with crack depth.



(a)



(b)

Figure 6.13 The results obtained in correlating frequency change with (a) crack surface area and (b) crack depth.

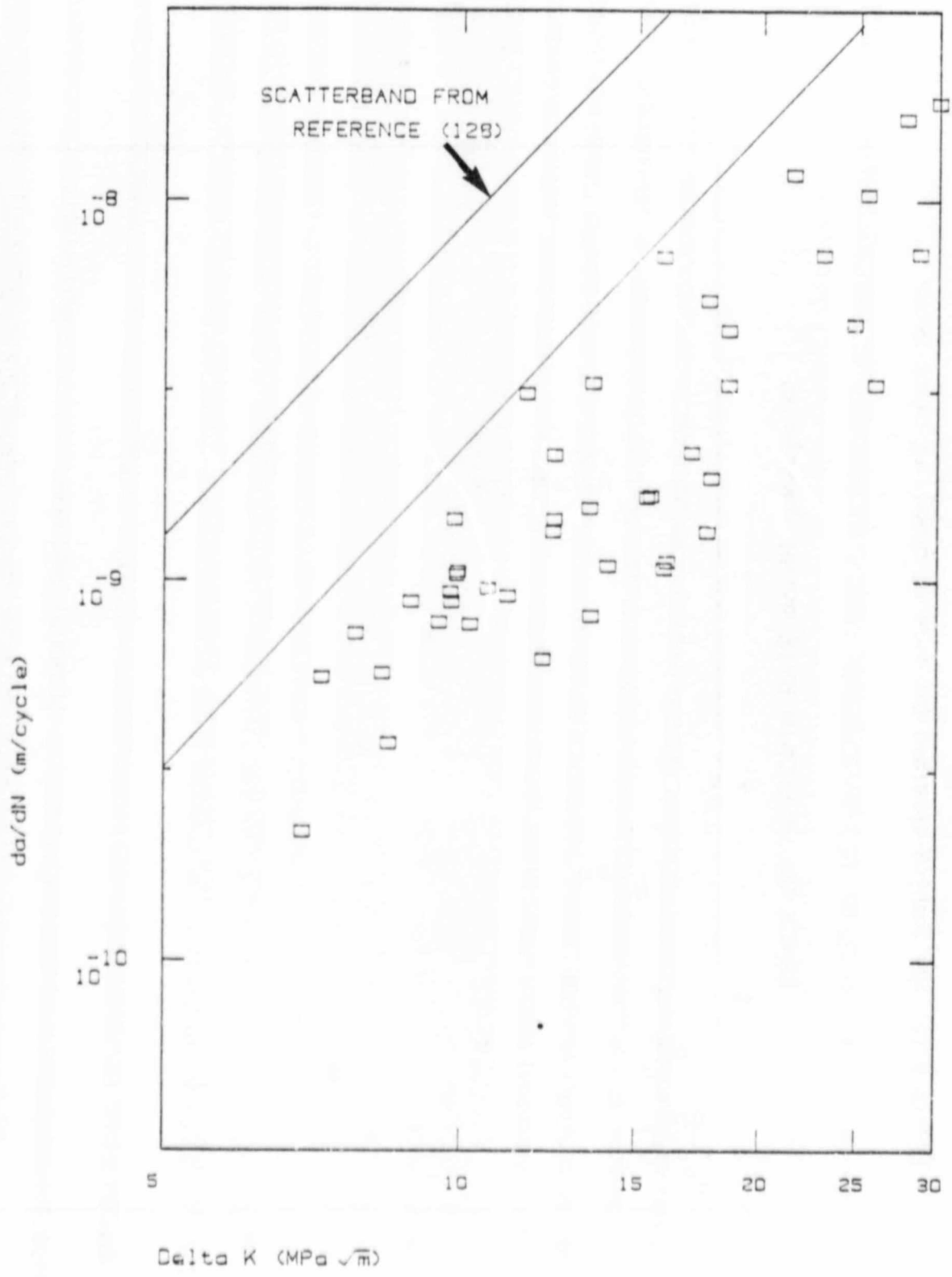


Figure 6.14 da/dN versus $\triangle K$ for beachmarked specimens. These crack tip stress intensities were calculated from (128).

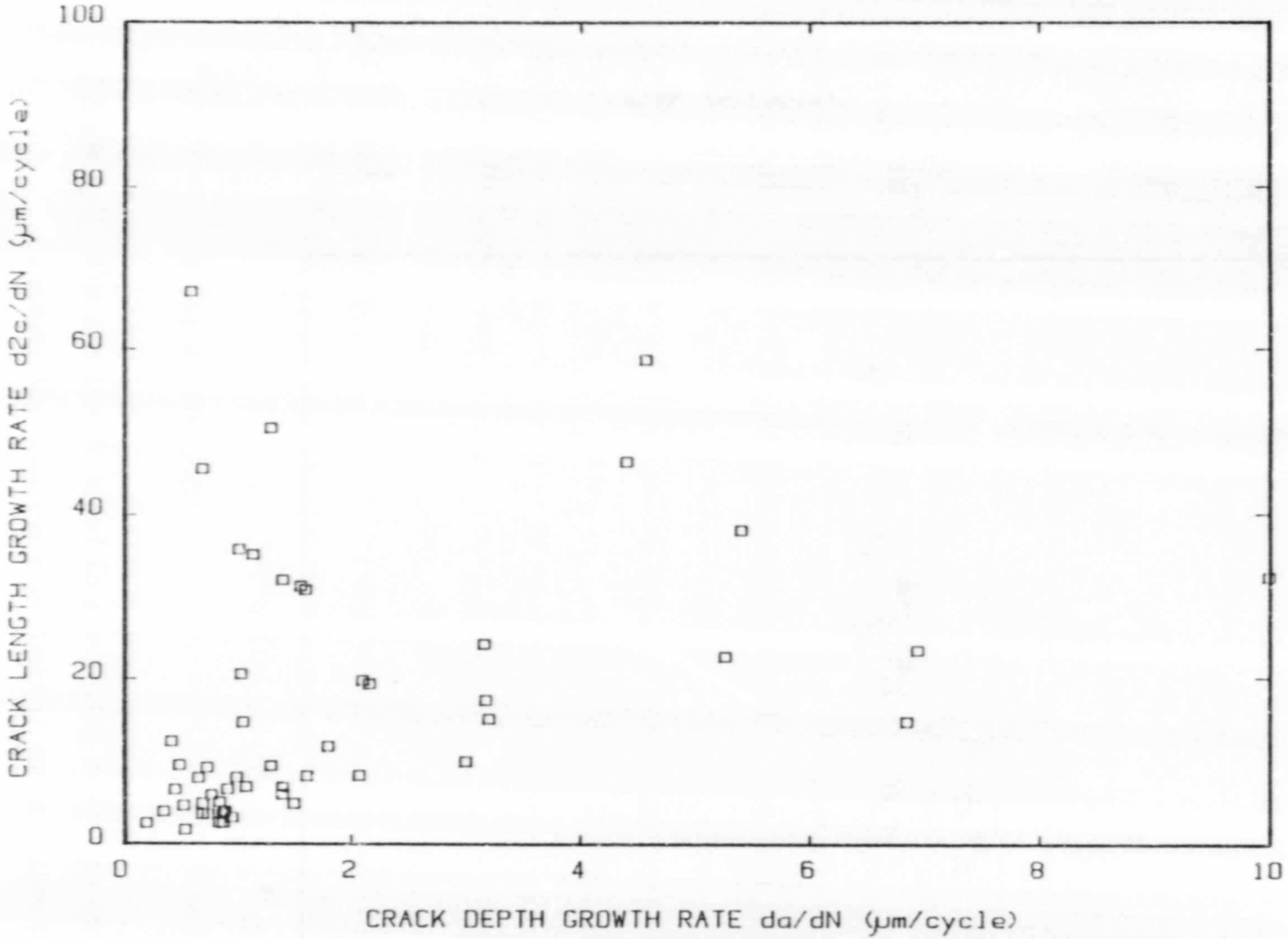


Figure 6.15 The results obtained for rate of change of crack depth (da/dN) compared with the rate of change of crack surface length (d2c/dN).

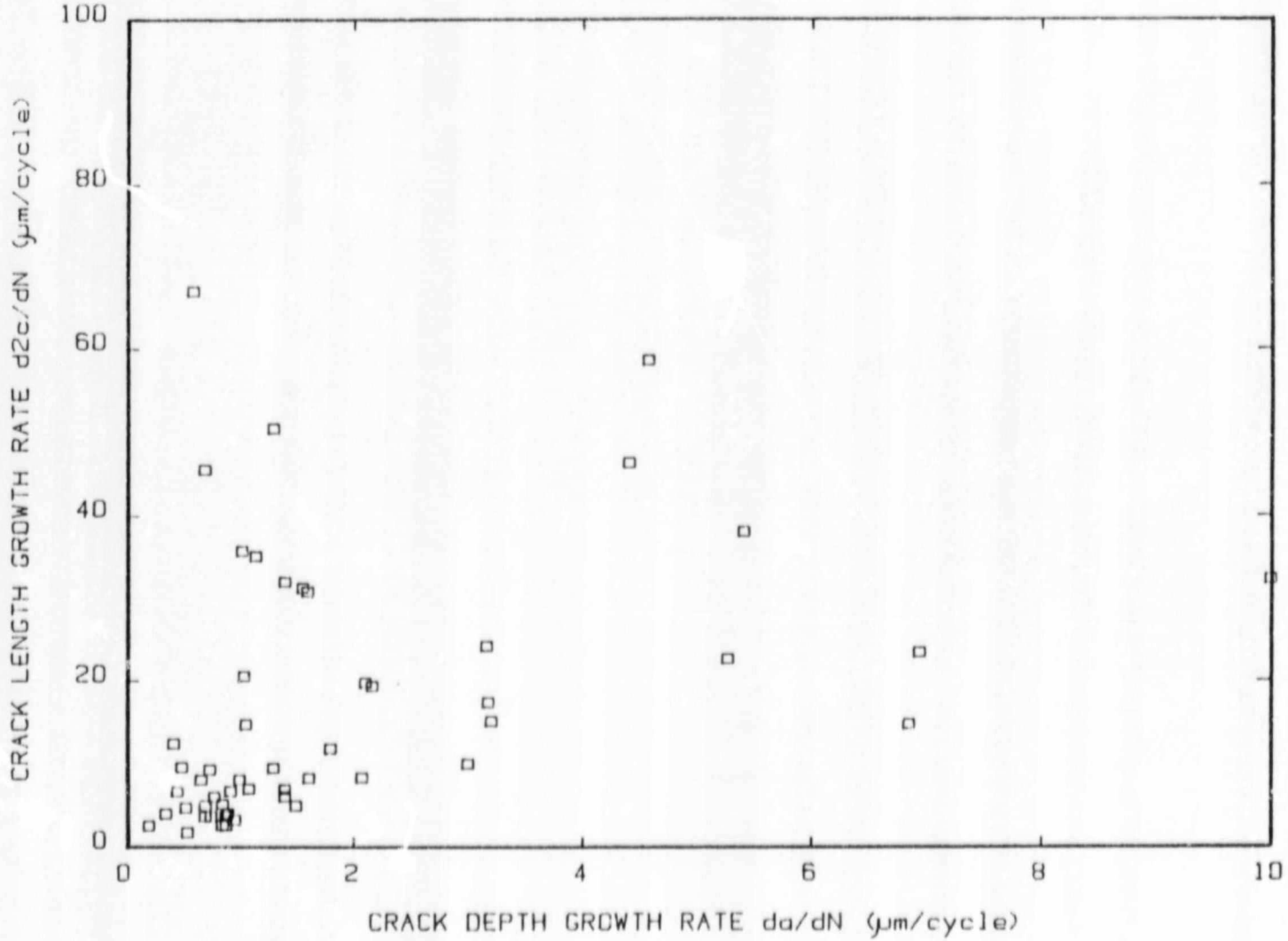


Figure 6.15 The results obtained for rate of change of crack depth (da/dN) compared with the rate of change of crack surface length (d2c/dN).

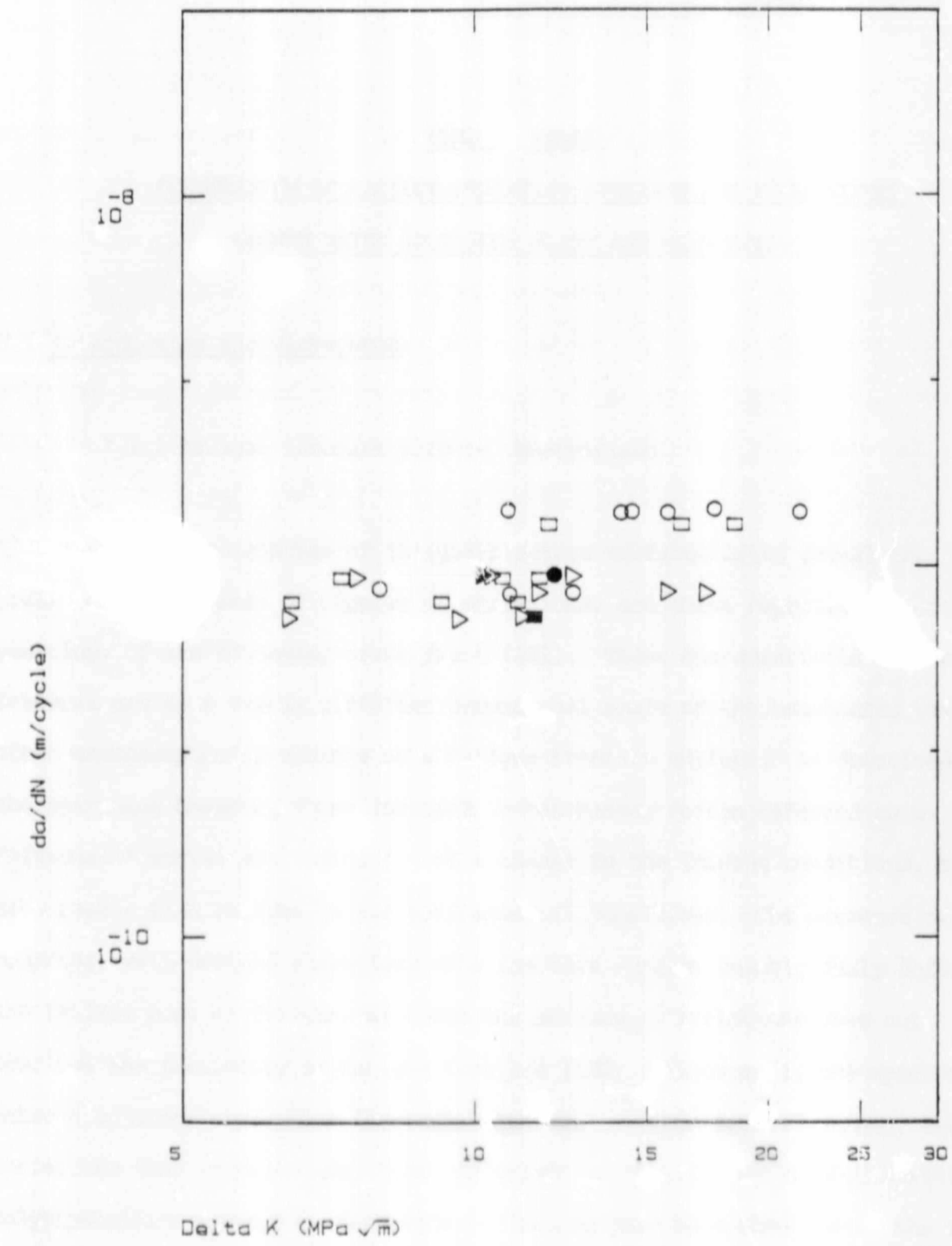


Figure 6.16 The results obtained in predicting crack tip stress intensities from the experimental correlations between crack depth and potential drop, and between crack depth and crack length. Each symbol type represents one potential drop reading, the open sybmols are calculated from the predicted crack parameters, the solid symbols are the actual results calculated from the beachmarks.

CHAPTER SEVEN

CORRELATION OF FATIGUE STRIATION SPACINGS AND MACROSCOPIC GROWTH RATES IN PARENT PLATE AND WELD METAL

7.1 Introduction and Background

7.1.1 Fatigue-fracture surface observations

High magnification studies of fatigue-fracture surfaces often reveal the presence of a pattern of ripples or striations, and these represent successive positions of the advancing crack front (132). These characteristic surface features are on a vastly different dimensional scale to the beachmarks that are often macroscopically visible on a fatigue fracture surface. As described in the preceding Chapter, these macroscopic beachmarks (often referred to as "clamshell" marks) are indicative of a change in the loading conditions, but may also result from changes in the environmental conditions. The presence of numerous, well-defined striations on a fracture surface unambiguously defines the failure mode as fatigue, although the absence of striations does not preclude the possiblity of fatigue fracture (132). In general, the spacing between adjacent striations increases with the level of applied stress, and the striations tend to curve away from the origin of the fatigue crack. However, in polycrystalline microstructures wide variations have been observed in the local orientation of the crack paths, as shown schematically in Figure 7.1 (133). An added complication is that the spacing of striations in adjacent fracture areas has also been shown to vary (132). The morphology of fatigue striations are also dependent on the type of alloy, and are more uniform in FCC alloys such as aluminium and austenitic stainless steels than in ferritic alloys.

Furthermore, it has been shown (see, for example, reference 134) that although one loading cycle can produce one striation, the converse is not always true

(24-28,132,134) i.e. one striation may not be produced by a single load cycle. This is due to the fact that at low applied stress levels the strain at the crack tip may be too small to produce an increment of crack extension for each applied load cycle, whilst at high applied stresses, the static failure modes contribute to crack extension (26,132). As discussed previously in Chapter Five, fatigue crack propagation may be enhanced by ductile (micro-void coalesence) or brittle (cleavage) extensions of the crack front; such fracture modes are predominant in situations where the applied stress is either due to a dead load (i.e. fully static conditions) or where the load monotonically increases with time. Clearly, ductile crack extension will occur in high toughness microstructures, and cleavage in low toughness microstructures.

The precise mechanism of striation formation has not yet been established, although it is widely accepted that it involves plastic blunting of the crack tip during the tensile portion of the loading cycle, and subsequent resharpening under compression (132-135). The most generally accepted of these models, due to Laird (136), is shown in Figure 7.2. However, it was shown that fatigue striations could not be resolved when the testing was carried out at growth rates less than 5×10^{-6} m/cycle under vacuum (134), and this would therefore tend to question the validity of the plastic blunting theory. An alternative model was proposed in which the crack extension progressed by alternating shear; the reversed slip would be blocked by a surface oxide film, but fully reversible in vacuum (134), thereby accounting for the disappearance of the striations. It was concluded (134) that Laird's model would be applicable at high growth rates (greater than 10^{-5} m/cycle) in vacuum. However, as a further illustration of the controversy apparent in the literature on this topic, fatigue striations <u>were</u> resolved in aluminium alloys tested in vaccuum at growth rates less than 10^{-7} m/cycle (28)!

7.1.2 Fracture mechanics and striation spacings

The correlation of fatigue striations with the number of loading cycles is an

important concept, since this may give some quantitative information with regard to the applied stress level. As discussed in Chapter Three, the concepts of fracture mechanics can be used to describe the likelihood of crack extension from a pre-existing defect under static load conditions, and it was further shown in Chapter Six that fatigue cracking from a weld toe could be described by the stress intensity at the crack tip. The relationship between the rate of crack growth (da/dN) and the cyclic stress intensity (ΔK) shows a typical sigmoidal curve, when plotted on a log-log scale, as shown in Figure 7.3. In this curve, the upper assymptotic limit is determined by the fracture toughness of the material, and the lower limit by the threshold stress intensity, K_{th}, below which crack propagation cannot be detected. In many practical situations, however, the fatigue crack growth rate does not aproach either of these two limits, and may be described by the Paris growth "law" (137):-

$$da/dN = A\ (\Delta K)^m \qquad (7.1)$$

In equation (7.1), A and m are material constants (m is also determined by geometry and environment), and these can therefore be evaluated by suitable testing. If equation (7.1) is integrated, it will be possible to evaluate the number of cycles required to grow a crack from an initial length, a_i (for example, the limit of the non-destructive testing method used) to a final length, a_f (the "critical" crack size for catastrophic failure). This will serve as a useful indication of the safe-life of the structure, as well as defining (with appropriate safety margins) the period of in-service inspections.

Clearly, if the striation spacing can be equated to the crack growth rate, da/dN, these microscopic features will serve as a useful evaluation of the cyclic stress intensity, ΔK. Thus, it should be possible to estimate the applied dynamic stress levels, provided the appropriate stress concentration factors and the geometrical correction factors are known. Thus, in the investigation of the causes of service failures (generally situations where the macroscopic growth rate has not been monitored), measurements of striation

spacings from the resulting fracture surfaces may enable the investigator to quantify the service stresses, and hence make recommendations for the avoidance of such failures.

However, the validity of such quantitative studies have been questioned, due in part to the the practical difficulties involved in the measurement of fatigue striations on a service fatigue fracture surface, (the least of which is the removal of any oxide layers on the fracture surface without affecting the underlying metal). A number of laboratory studies have been performed on the correlation between striation spacings and growth rates, in an attempt to establish whether or not this can be used with any confidence in estimating the applied stresses (see, for example references 25-27). However, as will be shown in the next Section, these results do not provide a definitive solution: indeed, the contrary findings serve to illustrate the need for further reserach in this area.

7.1.3 Correlations of striation spacing and macroscopic growth rate

The term "macroscopic growth rate" defines the incremental change in crack length with the number of applied loading cycles, as measured by optical microscopy, potential drop techniques or compliance methods. Clearly, while this may easily be measured in laboratory testing, it will not be feasible in most practical situations. Thus, correlations between fatigue striation spacings and macroscopic growth rates are, of necessity, carried out on laboratory test specimens.

A fractographic study performed on fatigue cracks obtained in aluminium alloys, tested at near threshold stress intensities, indicated the presence of both fine and coarse striations (28). The fine striations were seen to be subunits of the coarse striations, but could form in their absence, and were therefore considered to be more directly related to the incremental crack advance. Even the fine striation spacing, however, overestimated the actual crack growth rate,

as exemplified in Figure 7.4. It was therefore concluded that crack growth in this particular case was a two-stage process, crack extension could only occur after sufficient local strain had acummulated at the crack tip (28). At the low applied stress levels used in this investigation, a number of loading cycles were necessary to accumulate this required amount of strain.

As part of a study performed on the initiation and growth of fatigue cracks in notched mild steel specimens, it was shown that at low growth rates, the striation spacing would overestimate the actual crack growth rate, and underestimate it at high growth rates (26). This data is shown in Figure 7.5, and it is apparent that the "turning-point", or the crack growth rate at which the striation spacing begins to underestimate the actual growth rate is approximately 5×10^{-7} m/cycle. However, it is evident that there is a large degree of scatter in the striation spacings at all growth rates, and in addition, the data is rather sparse and therefore, possibly, inconclusive.

However, the striation spacing has been shown to correspond with the macroscopic growth rate in the mid-growth rate regime for AISI 4340 (EN 24) alloy steel and 18 Ni maraging steel (24); for type 403 stainless steel, A533 B steel, 7079 and 5456 aluminium alloys and Ti-6Al-4V titanium alloy (25); and for 7075 and 2024 aluminium alloys and Ti-6Al-4V titanium alloy (138). Figure 7.6 illustrates the correlation obtained in two of these studies, showing the dependence of both macroscopic growth rates and striation spacings as a function of the crack tip stress intensity. The results shown in this Figure again indicate that at low applied stresses, the striation spacing overestimates the rate of crack growth, but underestimates it at high levels of applied cyclic stress intensity. It is considered that the results shown in Figure 7.6 (a) are somewhat misleading, since the correlation appears to be excellent for most of the range of growth rates (25). Accordingly, this data has been replotted as striation spacing versus crack growth rate, as shown in Figure 7.7. This Figure clearly illustrates the actual scatter between the two parameters, and it can be seen that, at high growth rates (greater than 1.5×10^{-6} m/cycle) the striation

spacing is approximately half the actual growth rate, although there is a paucity of data for these growth rates.

Indeed, this study (25) concluded that the striation spacing is a function of the strain in the vicinity of the crack tip and could therefore be characterised by the equation:-

$$\text{Striation spacing} \simeq 5.4(\Delta K/E)^{2.1} \qquad (7.2)$$

This should be compared to the Paris growth "law" defining the Stage II crack propagation rate, detailed as equation (7.1) in the preceding Section, which was shown to be material dependent. From equation (7.2), it will be noted that material properties are accounted for by normalising the cyclic stress intensity (ΔK) with respect to the Young's Modulus, E.

More recently, in a fractographic examination of weld toe fatigue cracks, Albrecht (27) used periodic overloads to mark the fracture surface, and computed a "macroscopic fatigue striation spacing" as the distance between each successive overload, divided by the number of cycles between each overload. (It should be noted here that the term "striation" defines a microsopic feature.) These "macroscopic" fatigue striation spacings were then compared to a scatterband obtained from the literature (contained here as reference 54) for the corresponding microstucture, and as shown in Figure 7.8 (a), these "macroscopic" fatigue striations overestimate the band of crack propagation rate obtained from the literature. This was thought to be due to the different test conditions under which the two sets of data were obtained (27).

This study also measured the "microscopic" striation spacings using scanning electron microscopy, and Albrecht identified "quasi-striations", the spacing of which was an order of magnitude greater than the "observed" crack growth rate (27). However, these were located in the initial portion of the fatigue-fracture surface, and would therefore tend to confirm Jack's (26)

conclusion that at low growth rates, striation spacings will overestimate the actual growth rate. "Micro-striations" were measured in the final portion of the fatigue-fracture surface but again these were compared to the scatterband from the literature, as shown in Figure 7.8 (b). As can be seen in this Figure, the striation spacing was also compared to Bates and Clark's equation (reproduced earlier as equation (7.2)), but with no general agreement. Indeed, the results in Figure 7.8 (b) would tend to indicate that the striation spacing generally overestimates the crack growth rate.

It is most important to recognise that the actual macroscopic growth rate in these specimens was not rigorously evaluated, and therefore, these results (27) are essentially meaningless. Thus, the necessity for a more carefully performed test programme is evident from the critical appraisal of the results obtained from previous work in this field.

7.1.4 Crack front curvature and crack length monitoring

It will be appreciated that, in order to correlate macroscopic crack growth rates with striation spacing measurements, it is essential to identify precisely which portion of the fatigue-fracture surface that the striation measurements are made from. One of the prime difficulties in this excercise, however arises due to the fact that it is virtually impossible to grow a straight-fronted, through-thickness fatigue crack, with the result that the surface crack length measurements will tend to underestimate the crack length in the centre of the specimen. Thus, when scanning the center of a specimen, any crack curvature must be accounted for when calculating the crack length at which the fractographic studies are performed.

Crack front curvature is particularly evident when growing a fatigue crack in a welded sample where the residual stresses will affect the actual stress distribution in the specimen, and the crack length may be different on each side of the specimen. It will be recalled from Chapter Four that residual stresses

also arise from machining, and thus the preparation of a specimen for subsequent fatigue testing should be performed with some care. Obviously a further factor which can affect crack front curvature is any eccentric loading during the fatigue test. (This will not be an issue in a carefully designed test system, but can become important in practical situations.)

The bowed shape that occurs with Mode I loading is inherent in the method; as indicated in Chapter Six, the fatigue crack shape is determined by the loading arrangement as well as the specimen geometry. In a compact tension specimen, the edges are in a state of plane stress, whereas the centre, or mid-thickness is in a state of plane strain, and this is thought to be one of the factors which cause crack front bowing (139). There are certain methods of reducing bowed growth, including using a chevron starter notch such that the fatigue crack initiates at the tip of the chevron, or fully side-grooving of the specimen such that the near-surface stress fields are elevated, and the near-surface crack growth is enhanced. However, it should be noted that the crack front shapes achieved using a chevron notch are <u>not</u> conclusively less bowed than those initiating from a straight-fronted notch; in addition, full side grooving can cause reverse bowing such that the growth in the specimen mid-thickness is retarded (139).

Thus optical measurements of fatigue crack growth rate may not be entirely appropriate when performing a critical assessment of the correlation between the macroscopic growth rates and the associated fractographic features. The potential drop technique has, on the other hand, been shown to provide a "total" measurement, inclusive of crack curvature (124). Indeed, it has been shown for centre-cracked tension (CCT) specimens, single edge notched bend (SENB) specimens and compact tension (CT) specimens that the increase in potential with crack length can be equated using Johnson's solution (140). This only requires the initial and final crack lengths as input data, and the incremental increase in potential during the fatigue test may then be used to indirectly determine the change in fatigue crack length. However, as discussed in Chapter Six, since

the potential drop is an indirect method, it must be calibrated for the paticular specimen type under consideration. This can be done, as decribed in the previous Chapter, by performing programmed load changes during the propagation of the crack such that a series of beachmarks are formed on the fracture surface.

7.1.5 Summary

This Section has described the ripple marks or striations that may be found on a fatigue-fracture surface, and has shown that, although these indicate successive positions of the crack front, they may not have a one-to-one correlation with the observed macroscopic growth rates, in contrast to much "popular" opinion from the field of fatigue.

Studies have been performed in an attempt to correlate fatigue striation spacings with macroscopic growth rates; however, there are no definitive trends apparent in these results. It has been shown that plotting fatigue striation spacings on the conventional log-log da/dN versus ΔK graph may give misleading results, since this would tend to indicate that striation spacing measurements may indeed be used to estimate the appled stress levels. However, when these data are replotted as striation spacing against the macroscopic growth rate, the actual difference between these two parameters is made more apparent. These differences, however, do not provide a clear unambiguous picture, due in the main to the paucity of the data, and the scatter observed. This therefore indicates the need for a carefully performed, critical assessment of the relationship between fatigue striation spacings and macroscopic growth rates, such that this relationship could be used in practical situations. Thus, such experimental assessments must be carried out in materials of direct relevance, and in view of the fact that service fatigue failures of welded structures are invariably associated with the welds, the assessment should include the fractographic examination of welded samples.

Indeed, one of the primary motivations for such a study arose when striation spacings were measured from the fracture surface of a fan that failed in service (16). These results were used to estimate the service stress levels, and it was predicted that the cyclic stress amplitude was in excess of 100 MPa. However, these components are designed such that the dynamic stresses during normal service conditions are of the order of 20 MPa, and this was in fact confirmed when a similar fan was strain-gauged during operation (17). As detailed in Section 7.1.3, a comparison of fatigue striation spacings and applied stress intensity was made for laboratory tested welded specimens; however, the striation spacings were compared with a scatter band of macroscopic growth rates, obtained from the literature. It is clear that this study would have been more useful if the striation spacings were compared to the actual growth rates observed in the test specimens.

Finally, the problems associated with accurate macroscopic crack growth rate determination were outlined. Clearly, if the striation spacings are to be compared to the macroscopic growth rates with any confidence, the crack growth rate throughout the specimen must be accurately measured. This therefore indicates the necessity for an indirect method of crack length determination that would account for crack front curvature.

The following Sections in this Chapter detail the experimental procedures used and results obtained in an investigation of the relationship between striation spacings and macroscopic growth rates, at various levels of applied cyclic stress intensities, in parent plate and weld metal compact tension specimens.

7.2 Experimental Procedure

Eight compact tension (CT) specimens, 15mm thick, were machined from an equal double V butt weldment, fabricated from BS 4360 Grade 55E steel, using the Manual Metal Arc technique and high tensile E7018 electrodes. One set of four specimens was fabricated in such a way that the notch was located at the center

of the weld, and the subsequent fatigue crack propagation occurred in the weld metal, as shown in Figure 7.9. The other four specimens were fabricated such that the fatigue crack propagation occurred wholly in the parent plate.

All testing was carried out using a standard 50kN ESH servohydraulic machine; a universal joint was fitted in the loading train, so as to minimise load eccentricity, and therefore reduce crack bowing. Crack extension was monitored on both sides of the specimens using travelling microscopes, with a 7x magnification and verniers reading to 0,01mm. (Prior to testing, the specimens were polished such that the fatigue crack would be easily visible). In addition, a Gould constant current supply and a high resolution Fluke digital voltmeter were used to monitor the change in potential during each test.

Tests were carried out at an R-ratio of 0,1, and at a relatively low frequency of 10 Hertz, in order that machine control could be optimised. Each specimen was pre-fatigued such that subsequent crack extension would not be affected by the notch, and then a 0,7R beachmark was made, by increasing the minimum load to 70% of the maximum load. An initial stress intensity level was then chosen, and this was kept constant by reducing the loads every 500 or 1000 cycle interval, depending on the rate of crack growth. The crack length was measured on each side every 500 or 1000 cycle interval in order that the loads for the subsequent block could be calculated from the average of the two. (In addition these crack lengths were subsequently used to establish the crack growth rate and these were therefore recorded, along with the voltage across the crack at that point). For a constant level of applied stress intensity, the crack growth rate should remain constant; in actuality however, there was some variation, as will be detailed in Section 7.3.1 to follow. After a sufficient amount of crack extension (typically 3-5mm) had occurred at this stress intensity level, the specimen was again beachmarked, and a new level of constant stress intensity was chosen.

It will be recalled from Section 7.1.4 that crack front curvature (or uneven

crack growth) is more prevalent in welded specimens, and this was in fact observed in the first of the weld metal tests, as shown in Figure 7.10, which plots the change in surface crack lengths with the number of applied loading cycles. Obviously, this difference in the surface fatigue crack lengths resulted in a difference of stress intensity across the specimen (since the stress intensity is directly dependent on the crack length). Thus, the driving force at the crack tip is always less on the shorter side; and (assuming a homogeneous microstructure) the crack will always grow faster on the longer side, and the situation cannot rectify itself. It is considered that the residual welding stresses (which are not uniform across the section thickness) are the prime cause of the initial uneven crack growth. The corresponding results obtained for the first parent plate specimen are shown in Figure 7.11, and it is clear that the two crack lengths almost always coincide, and thus the fatigue crack propagation is the same on both sides of the specimen. The crack propagation rate may, of course, be different in the mid-thickness, depending on the amount of crack curvature. (In these two Figures, the position of the beachmarks, as measured from each side, are shown by the horizontal portions in the respective a versus N curves).

For each nominal stress intensity level, there were three different crack growth rates, corresponding to that calculated for each side, and that calculated from the potential drop measurements. The accuracy of the potential drop is illustrated in Figure 7.12, where the crack lengths recorded for each side, and that calculated from the potential drop measurements of the second weld metal specimen are plotted as a function of the number of the applied loading cycles. It can be seen that the crack curvature in this weld specimen is much reduced compared to that shown in Figure 7.10, thereby indicating that the crack bowing was a result of residual stresses rather than experimental technique. Clearly, the residual stress distribution will vary along the length of a weld, and can therefore be expected to vary from specimen to specimen. Additionally of course, there will be microstructural variations along the weld, and therefore, between specimens.

It would seem from Figure 7.12 that the potential drop consistently overestimates the crack length, but as will be recalled from Section 7.1.4, the potential drop provides a total measurement of crack length, inclusive of curvature. A five point average crack length was calculated for each of the beachmarks in this specimen, and it can be seen (Figure 7.12) that these coincide almost exactly with the potential drop crack lengths at those points.

At the end of the test, the fatigue-fracture surface of each of the specimens were prepared for examination in a Cambridge S4 scanning electron microscope. In view of the fact that the beachmarkings may not be easily visible at higher magnifications (although macroscopically visible), a grid was scribed on each specimen. In this way, it was easy to identify exactly which area was being examined at any stage during the fractographic investigation.

In order to improve the resolution of the image obtained in the scanning electron microscope, the specimens were tilted at an angle of 40° towards the detector. Thus the striation spacings measured from the fractographs were smaller than the true striation spacings since the fractographs represented a projected image. Therefore, the striation spacing measurements obtained from these fractographs were multiplied by 1,305 (the reciprocal of the sine of 50°) in order to assess the true spacing.

7.3 Results and Discussion

7.3.1 Macroscopic crack growth rates

As outlined in the preceding sectio[illegible]edding constant ΔK tests were performed on two weld metal specimens (W2 and W3), and on two parent plate specimens, P4 and P5. Initially, however, constant load tests were carried out on each of one of the weld metal and parent plate specimens, such that the stress intensity and crack growth rate increased with increasing crack length

Author Boothroyd Colin Allistair
Name of thesis Fracture Mechanics Analyses Of Static And Dynamic Failures Associated With Welding. 1986

PUBLISHER:
University of the Witwatersrand, Johannesburg
©2013

LEGAL NOTICES:

Copyright Notice: All materials on the University of the Witwatersrand, Johannesburg Library website are protected by South African copyright law and may not be distributed, transmitted, displayed, or otherwise published in any format, without the prior written permission of the copyright owner.

Disclaimer and Terms of Use: Provided that you maintain all copyright and other notices contained therein, you may download material (one machine readable copy and one print copy per page) for your personal and/or educational non-commercial use only.

The University of the Witwatersrand, Johannesburg, is not responsible for any errors or omissions and excludes any and all liability for any errors in or omissions from the information on the Library website.